DFT Research on the Dehydroxylation Reaction of Pyrophyllite 2. Characterization of Reactants, Intermediates, And Transition States along the Reaction Path

Esther Molina-Montes,[†] Davide Donadio,[‡] Alfonso Hernández-Laguna,[§] and C. Ignacio Sainz-Díaz*,[†]

Laboratorio de Estudios Cristalográficos, Instituto Andaluz de Ciencias de la Tierra (CSIC/Universidad de Granada), Avenida Fuentenueva s/n, 18002-Granada, Spain, Laboratory of Physical Chemistry, ETH Zurich, USI Campus, Via Giuseppe Buffi 13, CH-6904 Lugano, Switzerland, and Estación Experimental del Zaidín, Consejo Superior de Investigaciones Científicas (CSIC), C/Profesor Albareda 1, 18008-Granada, Spain

Received: February 5, 2008; Revised Manuscript Received: April 16, 2008

We delineate the dehydroxylation reaction of pyrophyllite in detail by localizing the complete reaction path on the free energy surface obtained previously by Car−Parrinello molecular dynamics and the implemented metadynamics algorithm (Molina-Montes et al. *J. Phys. Chem. B* 2008, *112*, 7051). All intermediates were identified, and a transition state search was also undertaken with the PRFO algorithm. The characterization of this reaction and the atomic rearrangement in the intermediates and products at quantum mechanical level were performed for the two reaction paths found previously: (i) direct dehydroxylation through the octahedral hole (cross mechanism) or between contiguous hydroxyl groups (on-site mechanism) and (ii) two-step dehydroxylation assisted by apical oxygens for each of the two steps. New intermediates were found and determined structurally. The structural variations found for all intermediates and transition states are in agreement with experimental results. The formation of these structures indicates that the dehydroxylation process is much more complex than a first-order reaction and can explain the wide range of temperatures for completing the reaction, and these results can be extrapolated to the dehydroxylation of other dioctahedral 2:1 phyllosilicates.

Introduction

Pyrophyllite is a dioctahedral 2:1 phyllosilicate in which a sheet of octahedrally coordinated Al cations is sandwiched between two sheets of linked SiO_4 tetrahedra. Each octahedral aluminum is bonded to the tetrahedral silicon via an apical oxygen and to an adjacent aluminum via two hydroxyl groups. This clay mineral is an important raw material for ceramics, glass, and refractory materials and is also involved in phenomenological geology processes as a pressure-transfer medium.

The dehydroxylation of pyrophyllite to pyrophyllite dehydroxylate involves water loss from a hydroxyl group that destabilizes and traps the proton from the adjacent OH group following the reaction $2(OH) \rightarrow H_2O + Or$. The remaining oxygen, Or, is referred as the "residual" oxygen and remains in a dehydroxylate structure where the Al cations are five-coordinate.[2] Solid-state NMR investigations of the thermally induced formation of pyrophyllite dehydroxylate and its high-temperature transformations have detected five-fold coordination of the Al sites.[3,4] Infrared (IR) spectroscopy [5,6] and X-ray diffraction[7] have also been used to study the structural changes in the clay mineral at high temperatures. In a recent IR spectroscopic work,[6] a new OH species was observed at 3690 and 3702 cm^{-1} in the temperature range of 550−900 °C, suggesting that the dehydroxylation of pyrophyllite might be a complex process including the presence of intermediates. Other IR studies have identified the appearance of silanol groups at 3715−3720 cm^{-1} at high dehydroxylation temperatures.[8] In addition, differential thermal analysis (DTA) of this dehydroxylation revealed a two-step process within the temperature range of 550−900 °C.[4] Evidence for a nonhomogeneous loss of H_2O in dioctahedral phyllosilicates was also found by Heller et al. by Mössbauer analysis of Fe-containing muscovite.[9] Guggenheim et al. used Pauling bond strength rules to explain the crystallographic structure of muscovite, the possible intermediates obtained upon loss of H_2O groups, and changing interactions of the Al−OH bond justifying the wide range of temperature of this reaction.[10] All of these studies together predict that there is a bimodal loss of H_2O involving dehydroxylation and the broad temperature interval. In contrast, Stackhouse et al. concluded that the activation energy for the dehydroxylation steps is the same and independent of the dehydroxylation state of neighboring atoms.[11] Our interest is to clarify these discrepancies in the mechanism of the dehydroxylation of pyrophyllite. In addition, several aspects of the process of thermally induced dehydroxylation, such as the mechanism, structural transformations, temperature range, and reaction rate, remain only partially understood.

Two possible reaction mechanisms have been proposed for the dehydroxylation reaction: (i) one that evolves the hydroxyl groups that are oriented toward the same octahedral hole, that is, crossing the octahedral hole,[12,13] and (ii) one that involves the hydroxyls oriented toward different octahedral holes, that is, on-site to two edge-sharing Al octahedra that share the hydroxyl groups implicated in the reaction.[10] An in-depth study of what happens in pyrophyllite at the atomic level in high-temperature environments is important and useful for optimizing its industrial applications.

A potential problem of such experimental studies is that the dehydroxylation process does not appear to occur uniformly

* To whom correspondence should be addressed. E-mail: cisainz@ugr.es.
† Instituto Andaluz de Ciencias de la Tierra.
‡ ETH Zurich.
§ Consejo Superior de Investigaciones Científicas.

10.1021/jp8010876 CCC: $40.75
Published on Web 06/19/2008

within a crystal and the proton interactions are complex. Therefore, quantum mechanical simulations based on density functional theory (DFT) were used in the early years to predict the crystallographic properties of these minerals,[14,15] particularly for the dehydroxylation reaction.[11,16] We recently carried out an exhaustive DFT study on different possible mechanisms of this reaction.[1] We found that the on-site and cross mechanisms are possible with similar activation energies, although the cross mechanism has a lower free energy than the on-site mechanism. Also, we found the assistance of apical oxygens in the reaction mechanism. Moreover, we found that partial and total dehydroxylation have the same energetic barrier (60 kcal/mol), matching the experimental data for muscovite of 59.8 kcal/mol.[17] Stackhouse et al. proposed an approximate energy barrier of 56 kcal/mol for the protonation of adjacent edge-sharing hydroxyl groups, but no transition state (TS) was localized.[11] Sainz-Díaz et al.[16] found a theoretical semidehydroxylate derivative, reproducing the FTIR spectroscopic bands of Wang et al.[6] In the present work, our aim was to characterize the structural transformations that take place along the different reaction paths of the dehydroxylation mechanisms. DFT ab initio geometry optimization and a transition state search were applied to identify the reactants, transition states, and intermediates of the dehydroxylation mechanisms.

Models and Methods

All calculations were performed using CPMD, version 3.9, a DFT code based on plane waves.[18] The energy cutoff for the plane-wave basis employed was 70 Ry, and we used the BLYP exchange correlation functional[19,20] in the generalized gradient approximation (GGA). Troullier−Martin pseudopotentials in the norm-conserving formalism were used to describe the nuclear core and inner electrons.[21] Brillouin-zone sampling was restricted to the Γ point.

The procedure for the ab initio Car−Parrinello MD simulations[22] was described in our previous work.[1] We used a time step of 0.12 fs and a fictitious electron mass of 800 au in the constant-volume, constant-temperature ensemble. Afterward, we applied metadynamics[23] in the extended Lagrangian form.[24,25] The sum of gaussians provides an estimation of the free energy surface (FES), and the resulting ground-state electron density distribution as a function of the nuclear coordinates defines a potential energy surface (PES), which, in turn, was used for geometry optimization of the critical points of the dehydroxylation reaction. In this way, we located reactants, intermediates, and transition states of the reaction paths of the different mechanisms. The metadynamic run was followed until the reaction was completed. When the dynamical reaction trajectories had been identified, we explored the topology of the free energy surface (FES) and estimated the structure of the critical points with thermodynamic integration.

Optimization of the wave function and ionic positions of the intermediates was achieved at 0 K using the method of direct inversion in the iterative subspace (DIIS).[26] We used a linear scaling method for TS search (saddle point of first order) based on the microiterative scheme using the partitioned rational functional optimizer (PRFO) implemented in the CPMD code,[27] by following eigenmodes of the approximated Hessian.[28] This partial Hessian (finite-difference Hessian matrix of the core degrees of freedom) obtained from the TS search was also used to calculate harmonic frequencies by finite differences of first derivatives. The critical points of the PES involved in all mechanisms of this reaction were confirmed by vibrational analysis implemented in the CPMD code.

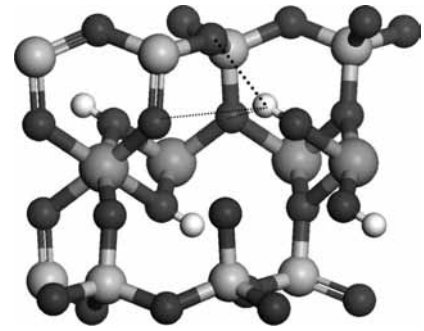

Figure 1. Pyrophyllite crystal structure and description of the main geometric features related to the OH groups. The Si, Al, O, and H atoms are represented in dark gray, gray, black, and white, respectively.

The experimental crystallographic data of pyrophyllite and its dehydroxylate derivative were used for the simulations and optimization calculations at constant volume.[2]

Results and Discussion

In this section, we describe and discuss the optimized structures of reactants, transition states, intermediates, and products with details about the geometrical features, lattice parameters, OH groups, and theoretical X-ray diffraction (XRD) patterns.

Two steps of the dehydroxylation reaction were investigated, coming from our previous work:[1] (i) the first step of the dehydroxylation reaction in which just one water molecule was formed in the octahedral ring and (ii) the second step dehydroxylation reaction starting from the semidehydroxylate derivative and removing the water molecule.

We characterized several reactants, transition states, and intermediates along the dehydroxylation mechanism paths. Specifically, we identified, for the first time, several semidehydroxylate intermediates for the on-site and cross mechanisms with and without water, the dehydroxylate derivative for the on-site and cross mechanisms with and without water, and the on-site and cross intermediates with the protonated apical oxygen. All of these structures were optimized at constant volume with the experimental lattice parameters of pyrophyllite (Figure 1).[2] Vibrational analysis of all of the optimized structures confirmed the minima (no imaginary frequency) and transition states.

With respect to the on-site derivative, the five-fold coordination of the aluminium atom forms a trigonal bipyramide in which one oxygen atom (residual oxygen, Or) is bridging between two pentacoordinated Al atoms (Al−Or−Al). In this intermediate, half of the Al−$(OH)_2$−Al groups are dehydroxylated alternatively, and the Al becomes five-coordinated. This is characteristic of the local on-site dehydroxylation mechanism,[10] and it corresponds to an Al−Al pair that has lost one bridging OH group, whereas the contiguous Al pair remains hydroxylated. On the other hand, the cross semidehydroxylate derivative also forms Al pairs in five-fold coordination, but the bridging residual oxygen remains protonated, giving rise to a residual hydroxyl group (OHr). The Al−OHr−Al pairs alternate with the contiguous six-fold Al pairs joined by an OH group (Al−OH−Al) and a residual oxygen (Al−Or−Al). This residual OH groups arise in the subsequent deprotonation to the formation of a second water molecule per unit cell that leads to complete dehydroxylation. Hence, the main structural difference between the semidehydroxylate intermediates of the two mechanisms is that, in the on-site derivative, the residual oxygen that joins the

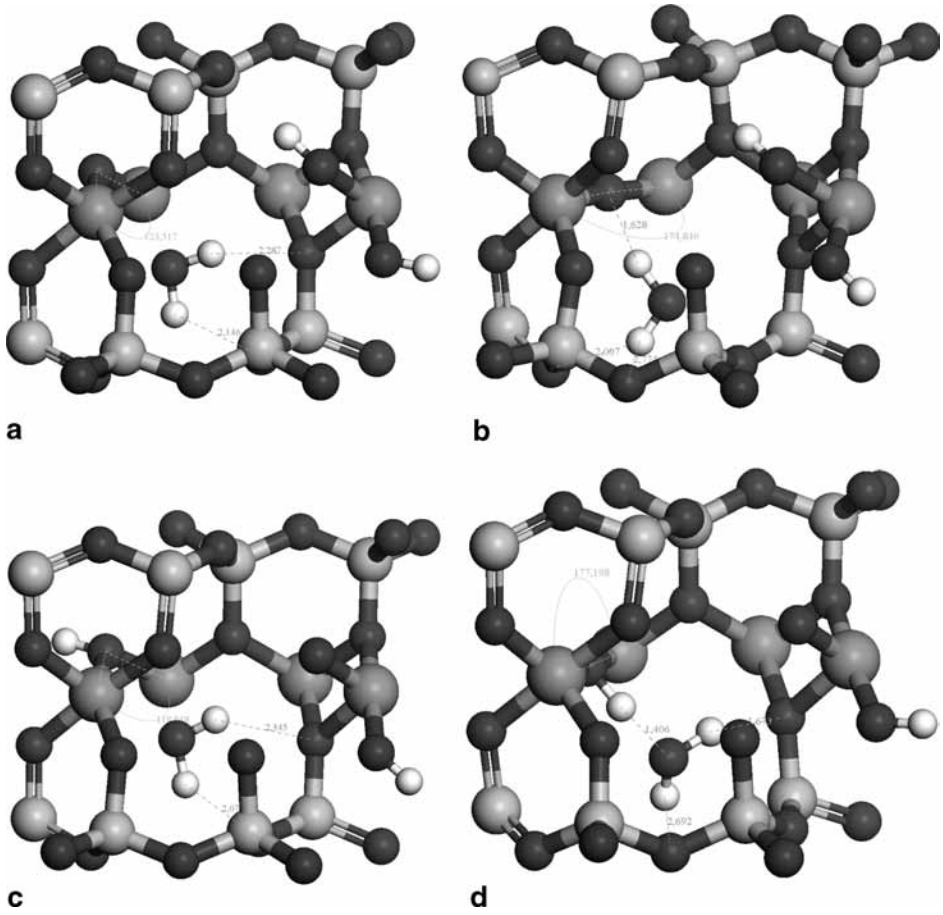

Figure 2. Interactions of the water molecule in the ditrigonal cavity in the optimized structures of the intermediates for the (a,b) on-site and (c,d) cross mechanisms. The Si, Al, O, and H atoms are represented in dark gray, gray, black, and white, respectively.

Al—Al dehydroxylated pair, Al—O—Al, is undersaturated with respect to positive charge (Figure 2a), whereas in the cross intermediate, the bridging residual oxygen is protonated and the undersaturation lies on the contiguous deprotonated oxygen (Figure 2c).

The structure of the completely dehydroxylated derivative is the same for both dehydroxylation mechanisms (on-site and cross), and again, the last water molecule can adopt a stable disposition in the ditrigonal cavity of the tetrahedral sheet, or it can be lost leading to the complete dehydroxylated structure characterized by Al—Al five-fold coordination pairs, which, in turn, form Al—Or—Al angles close to 180°, according to experiment (Table 1).[10]

Two variations on each intermediate exist: (i) on-site and cross intermediates with a water molecule in the ditrigonal cavity, which adopts two different configurations stabilized by hydrogen bonds with the surrounding oxygens (Figure 2a—d), and (ii) the same intermediates without the water molecule (Figure 3a and b). The completely dehydroxylated structure also exposes the derivative with and without the water molecule (Figure 3c and d, respectively). The main hydrogen bonds and O—H bond lengths of the water molecule in the ditrigonal cavity are shown in Figure 2. It is remarkable that the water molecule forms two types of hydrogen bonds depending on the configuration: (i) hydrogen bonds with the surrounding oxygens and (ii) hydrogen bonds with the residual oxygen or hydroxyl group. The global minima of these conformers are those depicted in Figure 2a for on-site intermediates and Figure 2c for cross intermediates. The secondary minimum of the on-site intermediate is that depicted in Figure 2b and has a higher energy (7.67 kcal/mol) than the global minimum. Even though the water molecule forms a very strong H bond with the residual oxygen, facilitating the formation of large AlOrAl angle, it is likely that electrostatic repulsions of the water oxygen with the surrounding oxygens (Figure 2b) can destabilize the structure of the second conformer, justifying its high energy, in contrast to the electrostatic attractions of the water oxygen with the Al cations in the global minimum (Figure 2a). The second minimum of the cross intermediate is that depicted in Figure 2d and has a much higher energy (39.0 kcal/mol) than the global minimum. In this second conformer, the OrH group forms a very strong H bond with the water oxygen, and one water hydrogen forms a strong H bond with one apical oxygen (Figure 2d); however, the electrostatic attractions of the water oxygen with the Al cations and the H bonds between the two water hydrogens with the surrounding oxygens can probably justify the lower energy of the global minimum (Figure 2c).

Geometrical Features. In Table 1, we report the main optimized geometrical features for comparison with the experimental values. The mean distances and angles measured in pyrophyllite match the experimental data with differences of less than 2%. These results are also consistent with recent DFT calculations of pyrophyllite, although the Si—O bond length calculated with CPMD is closer to the experimental value than those obtained in previous DFT calculations.[16]

In general, in the on-site intermediates, the changes in the atomic dispositions (Table 1) caused by the formation of a water molecule lead to a slight decrease in the mean value of the Al—O distance (from 1.943 Å in pyrophyllite to 1.930 Å in the semidehydroxylate with water and to 1.927 Å in the intermediate

TABLE 1: Main Geometrical Features of the Reactant and Intermediate Structures[a]

feature	pyro	on-site semi + H_2O	cross semi with H_2O	on-site semi	cross semi	dehydroxy with H_2O	dehydroxy	on-site apical	cross apical
Si—O	1.64 (1.62), 1.67[b]	1.64	1.65	1.65, 1.67[b]	1.64	1.64	1.65 (1.62), 1.67[b]	1.63, 1.72	1.64, 1.72
Al—O	1.94 (1.94), 1.94[b]	1.93	1.95	1.927, 1.91[b]	1.94	1.88	1.84 (1.82), 1.85[b]	1.97, 2.00, 2.39	1.94, 2.21, 2.25
Al—OH	1.89 (1.89), 1.90[b]	1.89, 1.72 (AlOr)	1.91, 1.76 (AlOr), 1.88 (AlOHr)	1.88, 1.68 (AlOr), 1.70[b]	1.91 (AlOH), 1.76 (AlOr), 1.85 (AlOHr)	1.69 (AlOr)	1.67 (AlOr) (1.80), 1.71[b]	1.91, 1.77 (AlOr)	1.89, 1.82 (AlOr)
d(Al···Al) (AlOAl)	2.96	2.92,[c] 2.98[d]	2.93, 3.00	2.93, 3.00[b]	2.91	3.33, 2.87	2.88−2.71 2.95[b]	3.30, 2.97	3.03, 3.19
d(Al···Al) (AlOHAl)	3.00, 3.03[b]	2.94, 3.04 (AlOrAl)	2.72 [M(OH)OrM], 3.24 (AlOHrAl)	2.94, 3.33 (AlOrAl), 3.40[b]	2.73, 3.54 (AlOHrAl)	3.27, 3.24[d]	3.342 3.41[b]	2.951, 2.78 (AlOrAl)	2.95, 2.73 AlOrAl)
d(Si···Si)	2.99 (2.99), 3.13[b]	2.93−3.07	2.94−3.05	2.91−3.11, 3.01−3.21[b]	2.92−3.05	2.87, 2.96, 3.1	2.95−3.16, 3.03−3.23[b]	2.95, 3.01	2.96, 3.01
θ(O—Si—O)	108.5	108.4	107.9	108.0	107.9	108.1	106.9	109.3	108.2
θ(AlOHAl)	103.1	102.3	90.8	102.9	91.5			101.8, 103.1	103.3, 93.1
θ(AlOrAl)		123.5	101.2, 118.8 (AlOHrAl)	168.3	101.7, 146.1 (AlOHrAl)	150.0,[d] 167.0[b]	179.4	92.4	98.7

[a] Mean values; distances in angstroms and angles in degrees. Experimental values for pyrophyllite[2] and dehydroxylate derivative[10] are in parentheses. Pyro, pyrophyllite; semi, semidehydroxylate intermediate; dehydroxy, dehydroxylate derivative; apical, intermediate with protonated apical oxygen. [b] Previous values from DFT calculations with basis sets based on atomic orbitals.[16] [c] Ditrigonal cavity of tetrahedral sheet without water. [d] Ditrigonal cavity with water.

TABLE 2: Characterization of the OH Groups in the Reactant and Semidehydroxylate Intermediates[a]

feature	pyrophyllite	on-site semidehydroxylate with H_2O	cross semidehydroxylate with H_2O	on-site semidehydroxylate	cross semidehydroxylate	protonated on-site apical oxygen	protonated cross apical oxygen
d(OH)	0.978 (0.977)	0.978, 0.979	0.976,[b] 0.983	0.979−0.977 (0.977)	0.979,[c] 0.987[d]	0.977,[e] 0.986, 0.979,[e] 1.004 (SiO—H)	0.978, 0.978, 0.979, 1.035 (SiO—H)
ρ(OH)	27.5 (33.0)	40.7, 9.3[f]	36.6,[c] 10.0[d]	33.9−33.0 (35.0)	47.5,[c] −10.8[d]	61.4,[e,g] −5.0,[g] 67.3, [c,e]	38.4,[e] 22.9
H_b	2.19 (2.10)	2.12, 2.37[f]	2.11,[c] 2.56[d]	2.15−2.06 (2.35)	1.98,[c] 3.34[d]	3.23,[e,g] 3.01,[g] 3.26[c,e]	2.06, 2.29
H_{a1}	2.69 (2.76)	2.76, 2.65[f]	2.80,[c] 2.60[d]	2.83−2.85	2.98,[c] 2.82[d]	3.04,[e,g] 2.35,[g] 3.08,[c,e]	2.88,[e] 2.59
H_{a2}	2.73 (2.86)	2.83, 2.64[f]	2.89,[c] 2.54[d]	2.84−2.98	3.10,[c] 2.88[d]	2.96,[e,g] 2.46,[g] 3.33,[c,e]	2.85,[e] 2.69

[a] Distances in angstroms and angles in degrees; values in parentheses from previous DFT calculations.[16] [b] OH oriented toward the layer with the water molecule. [c] Al(OH)OrAl group. [d] AlOHrAl. [e] OH oriented toward the ditrigonal cavity with the silanol group. [f] Oriented toward the cavity without water. [g] OH group from $Al(OH)_2Al$.

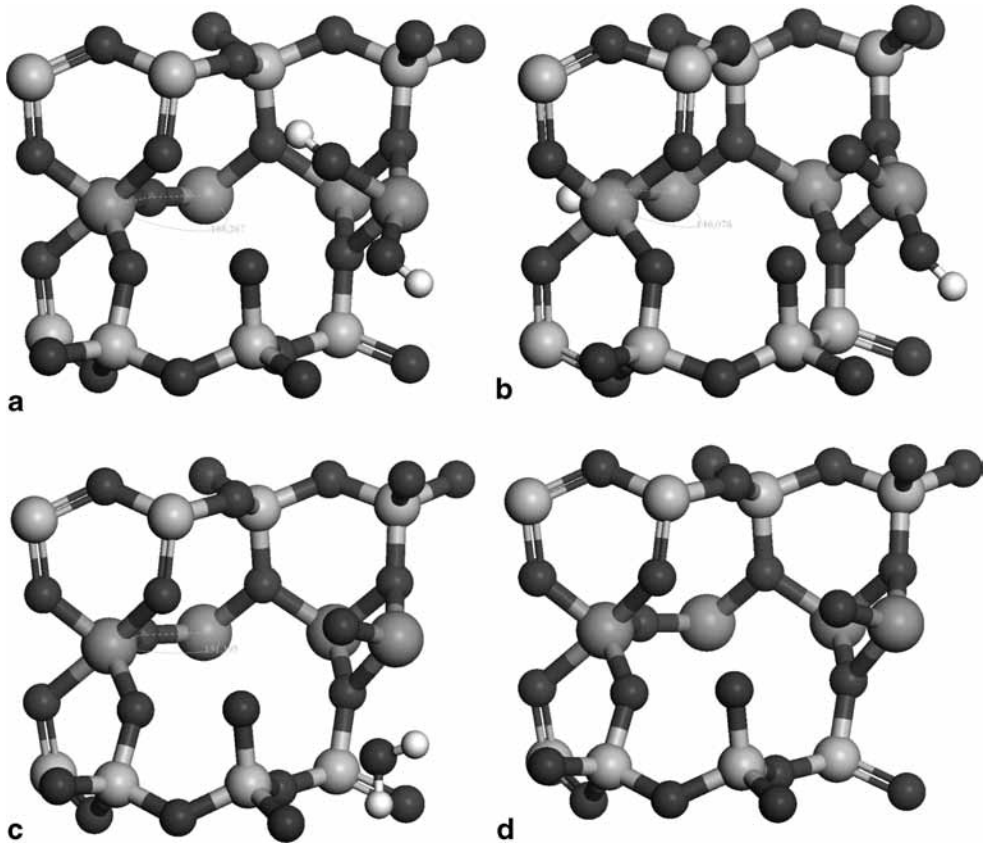

Figure 3. Semidehydroxylate derivatives without water for the (a) on-site and (b) cross intermediates. Dehydroxylate derivative (c) with water and (d) without water. The Si, Al, O, and H atoms are represented in dark gray, gray, black, and white, respectively.

without water). This effect is higher with the formation of the second water molecule after the second step of dehydroxylation with the same tendency, giving 1.88 and 1.84 Å in the dehydroxylates with and without water, respectively. In the cross semidehydroxylate intermediate, this distance is longer than in the on-site intermediate. In all cases, the release of water decreases the Al—O distance slightly. The hydrogen bonds of the water molecule with the O atoms compensate somewhat the charge defect produced by the water formation. This formation of water and pentacoordinated Al produces a defect of charge, so that the Al—O bonds become stronger, hence decreasing the Al—O distance. Although these differences are very small, this tendency is consistent with the conclusions of Guggenheim et al.[10] taken from experimental dehydroxylation studies along with Pauling bond strength calculations that also justify the formation of intermediates and the nonhomogeneity of the reaction.

Considering the Al—OH distance of the bridging Al—OH—Al unit, this distance is about 1.89−1.91 Å in pyrophyllite and all of the semidehydroxylate intermediates, whereas the Al—Or distance of the bridging Al—Or—Al unit decreases progressively, from 1.76 Å in the cross semidehydroxylate and 1.72 Å in the on-site semidehydroxylate with water to 1.68 Å in the on-site semidehydroxylate without water. According to Drits et al.,[7] in the Al five-coordinate prisms, the octahedral cation—Or distance becomes *b*/6, i.e., 1.51−1.52 Å, and this distance is too short for cations with pentagonal coordination. Therefore, the octahedral cations must move away from each other, as observed experimentally in dehydroxylated muscovite, for which the Al—Or distance is 1.69 Å[29] according to our calculations. In general, the release of water from the ditrigonal cavity produces a shorter Al—Or distance because the interactions between the O atom and the pentacoordinated Al cation become stronger and the Al—Or—Al angle increases. In the cross intermediate, these interactions justify the following sequence of Al—OH distances: d(Al—OH) > d(Al—OHr) > d(Al—Or), where the electron density is different in each case.

We found that the presence of water in the ditrigonal cavity generates interactions of the water molecule, with this bridging O atom affecting the Al—O bond length but also affecting the Al—Or—Al and Al—OHr—Al bond angles, which decrease in presence of water (123−118° in the semidehydroxylate intermediate with water, 168−146° in the semidehydroxylate intermediate without water, 150° in the dehydroxylate derivative with water, and 179.4° in the completely dehydroxylated structure). This is an important structural variation that was reported experimentally,[10] namely, the changes in the Al—OHr—Al angle, which varies from 103.1° in pyrophyllite to values near 180° as the reaction proceeds.

Another structural change is the progressive increase in the Al···Al distances. Two types of Al···Al distances can be distinguished: those between the Al pair involved in the dehydroxylation reaction and those between the rest of the Al pairs. Considering the first case, this Al···Al distance increases during the dehydroxylation reaction, forming the bipyramidal structure with Al pentacoordinated from 3.00 Å in pyrophyllite (Al—OH—Al) to 3.3 Å (AlOrAl) in the on-site semidehydroxylate intermediate and 3.34 Å (AlOrAl) in the dehydroxylate product, where the Al—Or—Al angle is close to 180°. A similar effect was observed with the cross intermediates. The presence of water in the ditrigonal cavity also affects this Al···Al distance, which is lower with water than without water, because this distance is related to the changes in the Al—Or—Al bond angle discussed above. In contrast, the rest of the Al pairs that

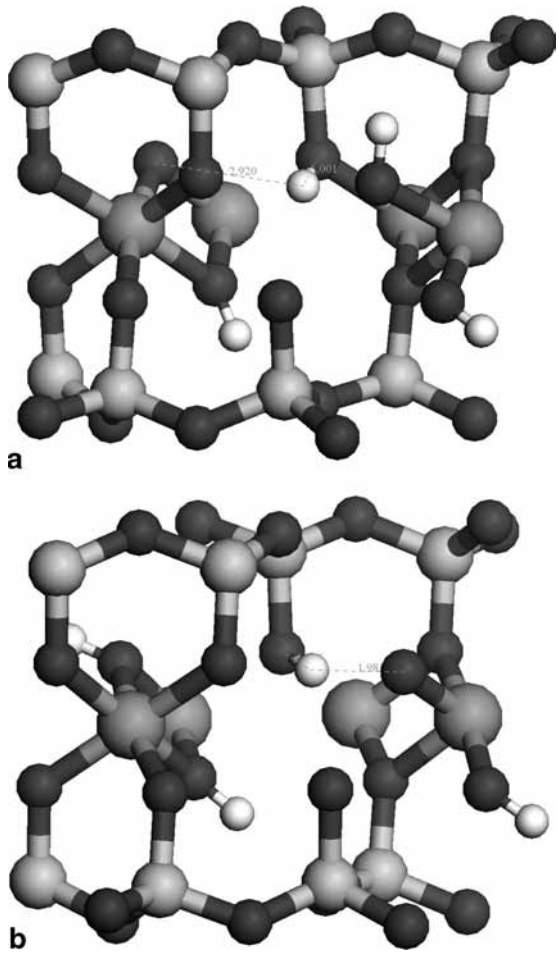

Figure 4. Apical oxygen intermediates: (a) on-site and (b) cross mechanisms. The Si, Al, O, and H atoms are represented in dark gray, gray, black, and white, respectively.

are not involved in the dehydroxylation tend to become slightly closer as the dehydroxylation reaction proceeds. The Al···Al distance in Al—Al pairs without OH groups (AlOAl) decreases from 2.96 Å in pyrophyllite to 2.93−2.91 Å in the semidehydroxylates and 2.87 Å in the dehydroxylate product. This decrease also occurs in the AlOHAl pairs that do not react as in the on-site semidehydroxylate (Table 1).

Some experimental IR investigations[6,30] detected that, during dehydroxylation, significant changes occur in the Si—Si interatomic distance, which increases from 2.98 to 3.03 Å. As a general rule, the silicate network of the tetrahedral layers is distorted as compared to the initial models. This was also observed in our case for all of the intermediate semidehydroxylated structures (Table 1).

The intermediate with a protonated apical oxygen appears in the two-step cross and on-site dehydroxylation mechanisms (Figure 4). The silanol group (Si—OH) was detected by IR spectroscopy during the dehydroxylation reaction,[8] but no reaction intermediate was proposed in that study. In this work, we propose such as intermediate. No significant difference in the main geometrical features was found with respect to the rest of intermediates. However, the presence of the silanol group produces some distortions in the OH groups and in the octahedra and tetrahedra, resulting in different values of the Al—O bond length and Al···Al distance (Table 1). The Si—O bond length of the protonated oxygen is longer (1.72 Å) than the rest of the Si—O bonds (1.63−1.64 Å). The distance of the H atom of the protonated apical oxygen to the residual oxygen is 2.71 Å in

TABLE 3: Geometrical Features of the Transition States (TSs) of the Dehydroxylation Mechanisms[a]

	on-site TS (TS_{OS})				cross TS (TS_{CR})		
geometrical features	$TS_{OS}1$	$TS_{OS}2$	$TS_{OS}1$	$TS_{OS}2$	$TS_{CR}1$	$TS_{CR}2$	$TS_{CR}2$
H···O_H aceptor	1.271	1.198	1.123	1.33	1.196	1.12	1.24
H···O_H donor	1.160	1.254	1.501	1.19	1.471	1.60	1.26
mean O—H	0.977, 0.978, 0.979	0.982	0.978	0.979	0.976, 0.98	0.98	0.98
mean Si—O	1.641	1.645	1.638	1.641	1.641	1.647	1.647
mean Al—O	1.86	1.91	1.84, 1.93, 1.97	1.84, 1.89, 2.02	1.79, 1.84, 1.99	1.92, 1.94, 1.99	1.85, 1.90, 1.99
mean Al—OH	1.88 (Al—OH) 1.770, 1.854 (Al—Or), 2.039	1.79 (Al—OH), 1.67 (Al—Or), 2.326	1.88, 1.94 (Al—OH), 1.79 (Al—Or), 1.95 (Al—OHr)	1.88, 1.92 (Al—OH), 1.76 (Al—Or), 2.03 (Al—OHr)	1.89 (Al—OH), 1.84 (Al—Or), 1.86 (Al—OHr)	1.88 (Al—OH), 1.84 (Al—Or), 1.88 (Al—OHr)	1.88, 2.03 (Al—OH), 1.77 (AlOr), 1.92 (AlOHr)
d(Al—O—Al)	2.88, 2.93	2.81, 2.86	2.93, 2.97, 3.07	2.92, 2.98, 3.00	2.97, 3.10, 3.01	2.97, 3.02, 3.17	2.90, 3.01, 3.11
d(Al···Al) (AlOHAl)	2.91, 3.41 (AlOrAl)	3.24, 3.32 (AlOrAl)	3.01, 2.85 (AlOrAl)	2.95, 2.88 (AlOrAl)	2.79, 3.19 (AlOHrAl)	2.94, 2.78 (AlOHrAl)	3.13, 2.69 (AlOHrAl)
d[Si—(O—H)—Al]	–	–	2.03, 2.47	1.97, 2.28	–	2.21, 2.33	2.03, 2.11
d(Si—O—Si)	2.90−3.10	2.91−3.07	2.94−3.02	2.90−3.02	2.92−3.15	2.93−3.12	2.92−3.06
θ(O—Si—O)	108.5	108.0	108.4	108.4	107.9	107.9	108.3
θ(Al—OH—Al)	101.3, 140.6 (AlOrAl)	127.9, 170.0 (AlOrAl)	103.5, 106.0 (AlOrAl), 94.2 (AlOHrAl)	102.0, 109.9 (AlOrAl), 90.4 (AlOHrAl)	95.3, 98.9 (AlOrAl), 118.2 (AlOHrAl)	103.0, 98.4 (AlOrAl), 95.1 (AlOHrAl)	106.1, 40.2 (AlOrAl), 45.5 (AlOHrAl)

[a] Distances in angstroms and angles in degrees. OS = on-site mechanism, CR = cross mechanism, $TS_{OS}1$ and $TS_{OS}2$ are the TSs of the first steps of dehydroxylation and complete dehydroxylation, respectively; TS_{OS2} and TS_{CR2} are the different TSs found for the on-site and cross mechanisms with apical oxygen assistance, respectively.

the apical on-site intermediate and 1.98 Å in the apical cross intermediate (Figure 4). Therefore, the shorter O···H distance of the latter intermediate shows a higher interaction and contributes to its higher stability, in agreement with our previous work.[1]

Characterization of OH Groups. Because the dehydroxylation reaction proceeds by the removal of hydroxyl groups from the octahedral sheet, we analyzed the geometry of these functional groups in the reactant and semidehydroxylate structures. For this analysis, we defined some geometrical features, including the OH bond length; the orientation angle (ρ) of the OH bond with respect to the (001) plane; and the main O···H nonbonding distances between the H atoms and the surrounding tetrahedral O atoms, namely, H_b with the basal O atom in front of the O—H bond and H_{a1} and H_{a2} with the apical O atoms of the tetrahedra that are in front of (Figure 1, Table 2). The additional H···O nonbonding distances surrounding the H atom are too long to be considered here.

All intermediates contain two types of OH groups: (i) one oriented toward the basal oxygen as the pyrophyllite OH groups and (ii) the other oriented toward the apical O atoms.

No significant difference in the O—H bond length was observed between pyrophyllite and the semidehydroxylates (0.976−0.979 Å). The OH from the AlOrHAl unit of the cross semidehydroxylate has a long OH distance (0.983 Å). The calculated ρ(OH) angle for pyrophyllite (27.5°) matches the experimental value (26−31.5°)[31] and is consistent with previous ab initio calculations (33.0°).[16] This angle is similar for the two OH groups in the on-site semidehydroxylate (33.0−33.9°), and it is slightly larger than in pyrophyllite. The presence of the water molecule in the ditrigonal cavity of this intermediate increases the ρ(OH) angle of the OH group (40.7°) that is oriented toward the same ditrigonal cavity, as a result of the repulsion between the two H atoms. In contrast, another OH group that is oriented toward the cavity without water does not maintain the same ρ(OH) value as the on-site semidehydroxylate (33−34°) but rather has a ρ(OH) angle of 9.3°. This OH is oriented toward the AlOrAl group. The AlOrAl angle is lower in the intermediate with water (123.5°) than in that without water (174.8°), and therefore, the interactions of this bridging residual oxygen with the H atom of the OH group are shorter than in that without water, justifying the low ρ(OH) value. This angle value means that the H_b distance is longer and the H_{a1} and H_{a2} distances are shorter than in the other OH group with the higher ρ(OH) value. In the cross semidehydroxylate intermediate, the OH groups have very different ρ(OH) values from each other because they are in completely different environments: one is an AlOHrAl group, and the other one is an Al(O)(OH)rAl group. The AlOHrAl group has a very low ρ(OH) angle even with a negative value (−10.8°), whereas the other one has a higher value (47.5°). These ρ(OH) values change the nonbonding distances H_b, H_{a1}, and H_{a2} significantly. In the presence of water, this cross intermediate shows a similar effect but the differences are smaller.

For the intermediates with the protonated apical oxygen, the SiO—H bond is oriented perpendicularly with respect to the (010) plane. In the on-site derivative, the SiO—H bond (1.004 Å) is balanced among the surrounding oxygens, whereas in the cross derivative, this H atom is oriented slightly toward the AlOr(OH)Al residual oxygen, and the SiO—H bond length is greater (1.035 Å). This long SiO—H bond in the cross intermediate could explain why the subsequent deprotonation of the apical oxygen during water molecule formation proceeds more easily through the cross mechanism than through the on-site mechanism. In general, the d(OH) bond lengths (0.977−0.979 Å) are similar to those of previous intermediates, except in the OH group that is not oriented toward the silanol group in the on-site derivative and shows a long d(OH) bond (0.986 Å). This OH group is oriented toward the AlOr(OH)Al residual oxygen, and the electrostatic interactions between the two atoms can justify this OH bond length, as well as the low value of ρ(OH) (−5°), the high value of H_b (3.01 Å), and the low values of H_{a1} (2.35 Å), and H_{a2} (2.46 Å) for this OH group. In the cross intermediate, this OH group is also oriented toward the silanol group, and the repulsion with this group decreases the interaction with the AlOr(OH)Al residual oxygen, so that d(OH) is not as long but is similar to those of the rest of OH groups. In the on-site intermediate, the OH groups oriented toward the silanol group have a very high ρ(OH) value (61.4−67.3°) because of the electrostatic repulsions between the H atoms of the two OH groups and the silanol groups in the same ditrigonal cavity (Figure 4a). These high ρ(OH) values justify the large values of H_b, H_{a1}, and H_{a2} for these OH groups. In the cross intermediate, the OH group oriented toward the silanol group has a lower ρ(OH) value (38.4°) than in the on-site intermediate, because the interaction with the silanol hydrogen is lower and there is only one OH in the ditrigonal cavity with the silanol group instead of two OH groups as in the on-site case. The ρ(OH) values for the rest of the OH groups in the cross intermediate (23°) are similar to the pyrophyllite ones.

Transition States. For the transition states, we analyzed the same geometrical features as above, and mainly the $H\cdots O_H$ donor and $H\cdots O_H$ acceptor distances in order to distinguish the main mechanisms (Figures 5 and 6, Table 3). The structural variations along the reaction paths on the Al—OH and Al—O distances are similar to the intermediates. The force analysis of all of the transition states (TSs) shows one imaginary frequency, confirming the TS character.

In the on-site mechanism, we can consider the TS structure of the simple mechanism for the formation of the semidehydroxylate intermediate ($TS_{OS}1$) and for the second step of dehydroxylation and formation of the complete dehydroxylate product ($TS_{OS}2$) (Table 3). The latter TS was optimized using the experimental cell parameters of pyrophyllite ($TS_{OS}2$) and of the dehydroxylate, and no significant differences in the geometrical features were observed. In $TS_{OS}1$, the delocalizing proton is 1.271 Å from the acceptor outgoing oxygen atom for water molecule formation and 1.160 Å from the donor oxygen, whereas in $TS_{OS}2$, the distance from the proton to the acceptor oxygen is smaller (1.20 Å). In $TS_{OS}1$, the outgoing OH group is oriented toward the interlayer space, perpendicular to the 001 plane, thus maintaining the initial OH bond length (0.979 Å and 0.977−0.978 Å for the OHs of the other Al—Al pair). This outgoing OH group can be considered completely separated from one of the initial Al atoms, $d(O\cdots Al) = 2.77$ Å; however, it still maintains a short distance with the other Al atom (2.039 Å). Therefore, one Al cation has five-fold coordination with d(Al—Or) = 1.770 Å, whereas the other Al cation still has six-fold coordination with d(Al—Or) = 1.854 Å. If we consider the reaction coordinates as H···O (donor/acceptor) distances and take into account the fact that the reaction is endoergic, the TS structure is closer to the reactant than to the product, which looks like it does not fulfill the Leffler−Hammond principle.[32,33] However, including the H—O (donor) orientation angle in the reaction coordinate, which changes from 123.9° in the reactant to 77.5° in $TS_{OS}1$, adds a bending normal coordinate to the transition vector, making it closer to the product than to the reactant. With this reaction coordinate, a more complex

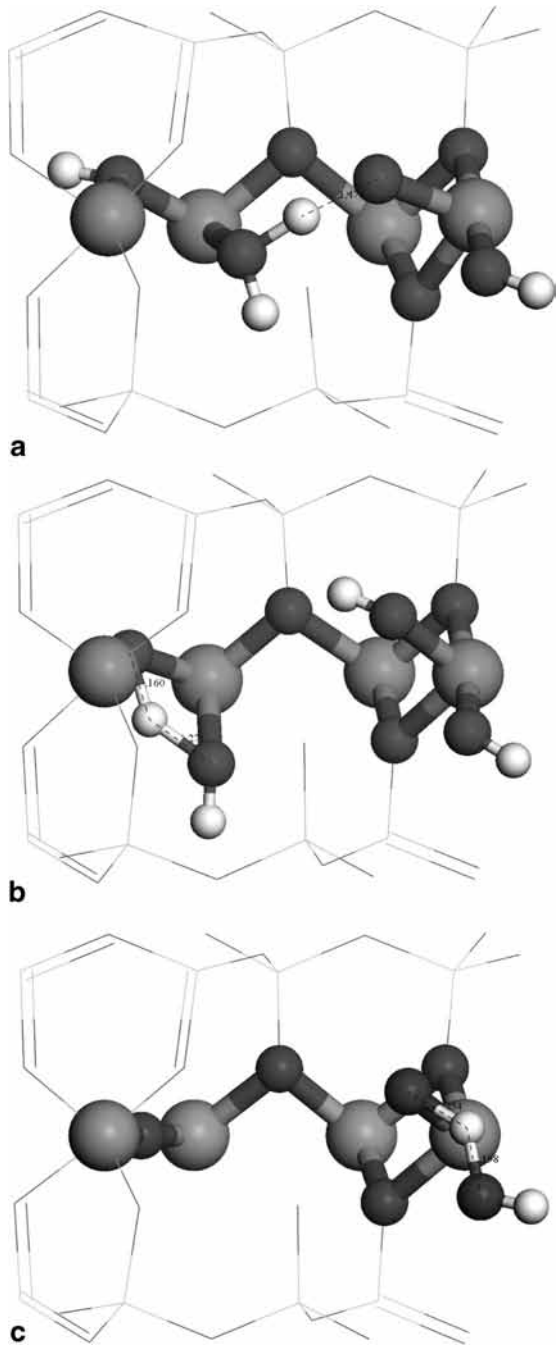

Figure 5. Transition states for the dehydroxylation reaction: (a) cross mechanism, (b) on-site mechanism, and (c) second on-site dehydroxylation step. The Si, Al, O, and H atoms are represented in dark gray, gray, black, and white, respectively.

reaction is found, in such a way the Leffler−Hammond principle is fulfilled. Therefore, the TS coordinate is based mainly on the migration of the H atom and the breaking of the remaining Al−O bond.

For the second step of dehydroxylation by the on-site mechanism, in $TS_{OS}2$, the outgoing OH group is equidistant between the two Al cations, $d(Al\cdots O) = 2.326$ Å, which can be considered pentacoordinated Al, $d(Al-Or) = 1.79$ Å. Therefore, the TS coordinate is based mainly on the migration of the H atom, in features similar to $TS_{OS}1$.

Regarding the TS of the cross mechanism ($TS_{CR}1$), the donor oxygen−proton ($O_H\cdots H$) distance is 1.47 Å, whereas the acceptor−proton distance is 1.196 Å. This TS shows a structure closer to that of the product, as it corresponds to an endoergic reaction, which agrees with the Leffler−Hammond principle; thus, only the H···O (donor/acceptor) distances can be considered as its reaction coordinate, which are much simpler than the reaction coordinates of $TS_{OS}1$ and $TS_{OS}2$. This simplicity in the reaction coordinate with respect to the on-site mechanism, even though the bending vibration corresponding to the orientation angle of the OH is a soft vibration; the relatively clear environment in the octahedral home for the cross mechanism with respect to the on-site mechanism; and the ergicity features make the cross mechanism much more favored than the on-site mechanism.

For the case of the apical oxygen mechanism, two transition states are observed: (i) one that corresponds to apical oxygen protonation for the on-site ($TS_{OS2}1$) and cross ($TS_{CR2}1$) mechanisms and (ii) one that corresponds to apical oxygen deprotonation toward water formation, also for the on-site ($TS_{OS2}2$) and cross ($TS_{CR2}2$) mechanisms. The distances of the delocalizing proton from the donor and acceptor oxygens are similar for the two mechanisms. In particular, deprotonation of the apical oxygen toward water molecule formation is given by an acceptor−H distance of 1.33 Å in the on-site intermediate ($TS_{OS2}2$) and 1.24 Å in the cross intermediate ($TS_{CR2}2$). On the other hand, these transition states are characterized by the bond breaking of the silanol−aluminum group (Si−OH−Al), which adopts a distance of 2.47 Å in the on-site mechanism ($TS_{OS2}1$) and 2.33 Å in the cross mechanism ($TS_{CR2}1$). The distorted Al arrangement in this localization remains until the water molecule is formed in the subsequent reaction step. In the first TS, the H···O (donor/acceptor) distances are lower than those in the product, corresponding to an endoergic reaction, again following the Leffler−Hammond principle. However, in the second TS, some differences are found in both the on-site and cross mechanisms. Considering the silanol intermediates as reactants in the former mechanism, the geometry of the TS is closer to that of the reactant as it corresponds to an exoergic reaction. Nonetheless, in the cross mechanism, the geometry of the TS is nearly symmetric, as it corresponds to a slightly endoergic reaction, which has a structure at the approximate midpoint of the reaction coordinate.

Crystal Lattice Parameters. We also performed geometry optimization with variable cell parameters. The optimized cell parameters are reported in Table 4 for comparison to the experimental data[2,10] in which the transition from pyrophyllite to its dehydroxylate leads to an increase of the *a*, *b*, and *c* lattice parameters. Drits et al.[7] noted that the main reason for the increase of the *b* parameter for dehydroxylated Al-rich 2:1 layers is a tendency for octahedral cations to move away from each other along the *b* axis to increase the Al−Or distance to an appropriate equilibrium value, and this is the main reason for the larger *a* and *b* parameters compared to original values. Experimentally,[10] a similar effect was observed that, during this thermally induced process, changes in the cell parameters occur, increasing the *b* parameter.

The calculated values for pyrophyllite are similar to the experimental results, except that the *c* parameter is slightly higher than the experimental value according to that previously reported in other DFT plane-wave calculations.[11,34] This is due to restrictions of DFT plane-wave calculations on van der Waals interactions presented in the lattice.

The semidehydroxylate intermediates found in our simulations were also optimized with variable cell parameters (with and without H_2O, cross and on-site). All of these semidehydroxylates present similar lattice parameters and are close to the experi-

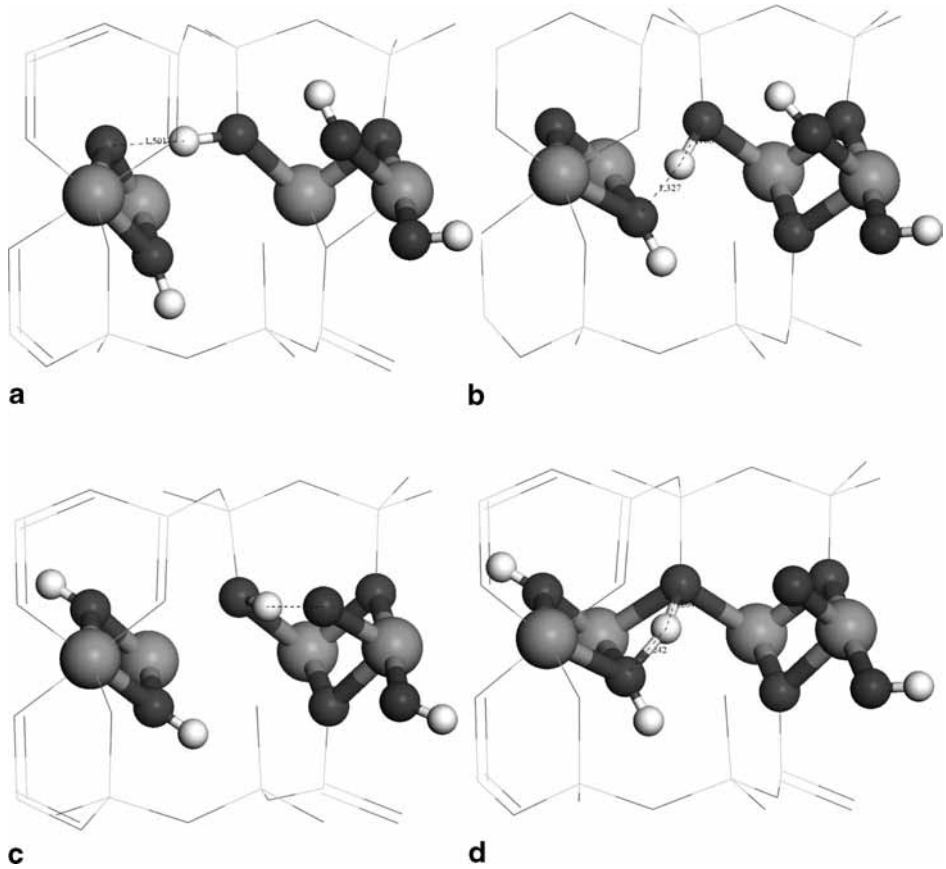

Figure 6. Transition states for the dehydroxylation reaction with apical oxygen assistance: (a,b) on-site mechanism [(a) apical oxygen protonation, (b) water molecule formation], (c,d) cross mechanism [(c) apical oxygen protonation, (d) water molecule formation]. The Si, Al, O, and H atoms are represented in dark gray, gray, black, and white, respectively.

TABLE 4: Lattice Cell Parameters of the Optimized Structures for the Reactant and Intermediate Structures[a]

cell parameter	pyro	semidehydroxylate on-site with H_2O	semidehydroxylate cross with H_2O	semidehydroxylate on-site	semidehydroxylate cross
a (Å)	5.18	5.21	5.20	5.20	5.20
b (Å)	9.01	9.08	9.02	9.08	9.04
c (Å)	9.79	9.77	9.81	9.82	9.81
α (deg)	90.6	90.8	90.79	90.6	90.9
β (deg)	100.2	100.1	100.1	100.2	100.1
γ (deg)	89.8	89.9	90.0	89.4	89.1

[a] Experimental data: For pyrophyllite,[2] $a = 5.16$ Å, $b = 8.97$ Å, $c = 9.35$ Å, $\alpha = 91.2°$, $\beta = 100.5°$, $\gamma = 89.6°$. For pyrophyllite dehydroxylate,[10] $a = 5.19$, $b = 9.12$, $c = 9.50$, $\alpha = 91.2°$, $\beta = 100.2°$, $\gamma = 88.6°$.

mental values for the dehydroxylate derivative, except for the b and c parameters. The c parameter is higher than the experimental value for the dehydroxylate derivative but closer to the experimental data than previous works on pyrophyllite with plane-wave DFT calculations.[11] The b parameter is slightly lower than the experimental value for the dehydroxylate derivative because the Al—O—Al bond angle of the pentacoordinated Al is lower than 180° and the Al···Al distance is shorter in the semidehydroxylate derivative than in the completely dehydroxylated structure. The presence of water in the ditrigonal cavity does not alter the lattice parameters.

X-ray Diffraction Pattern. Simulations of the powder X-ray diffraction (XRD) patterns of the calculated structures were performed using diffraction software implemented within Cerius2 package and XPowder software[35] with an X-ray wavelength of 1.54 Å. The simulated powder X-ray diffraction patterns based on the optimized structures of different semidehydroxylate intermediates (with water and without water) of the on-site and cross mechanisms are depicted in Figure 7. The range of 5−50° (2θ units) was considered for comparison. No significant differences were found between the semidehydroxylate derivatives and pyrophyllite. Slight differences can be detected between the semidehydroxylate intermediates without water molecules and pyrophyllite, but these differences are not observable within the experimental resolution. This can explain the fact that these intermediates cannot be detected experimentally by means of the XRD technique during the dehydroxylation process.

Conclusions

Several intermediates of pyrophyllite dehydroxylation were identified in this work: the semidehydroxylates with water (on-site and cross); the semidehydroxylates without water (on-site and cross), which are simultaneously the reactants of the second dehydroxylation step; and the completely dehydroxylate derivatives with and without water. This article also reports for the first time the apical oxygen intermediate that is consistent with the possible silanol group that was detected experimentally and assigned to a possible intermediate.[8]

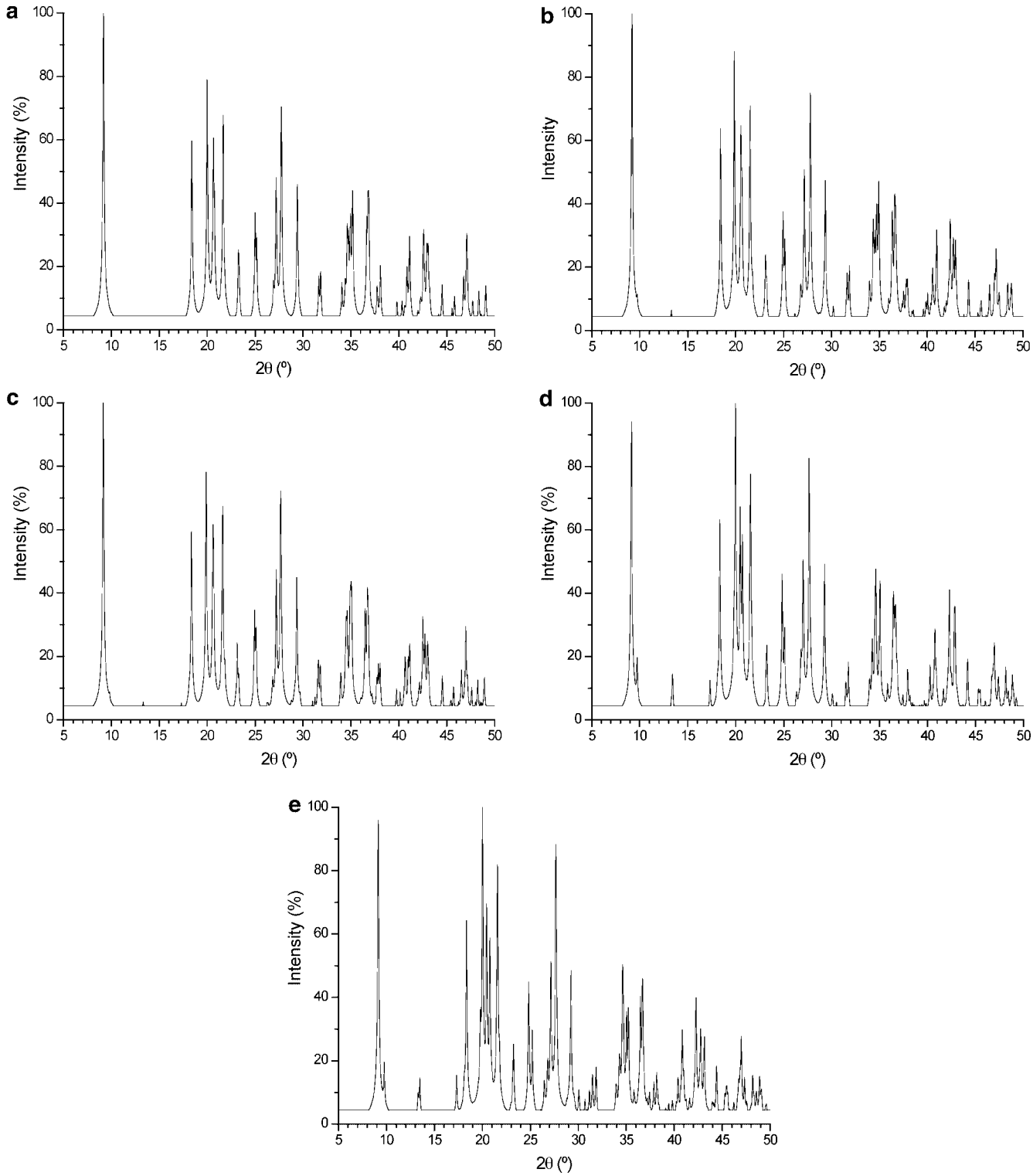

Figure 7. Simulated XRD patterns of the calculated crystal structures of (a) pyrophyllite, (b) semidehydroxylate on-site with water, (c) semidehydroxylate cross with water, (d) semidehydroxylate on-site without water, and (e) semidehydroxylate cross without water.

Variations observed in our calculated structures are in agreement with experimental findings such as five-fold Al coordination with a residual oxygen midway between the Al pairs. The simulation of the XRD pattern from our calculated crystal structures shows good agreement with the known experimental data. In addition, the similarity in the simulated XRD patterns of the intermediates explains the significant experimental difficulty in following the development of the reaction by XRD. This validation of our calculations and models shows that this theoretical methodology is a useful tool for analyzing intermediates and TSs for reactions in minerals that cannot be observed experimentally and can help to increase the understanding of the experimental behavior.

According to our previous results,[1] it is important to note that dehydroxylation would proceed with a higher activation energy only to favor the completeness of the dehydroxylation reaction. The conclusion of Guggenheim et al.[10] based on the gradual strengthening of the Al—O bonds along the intermediates of reaction are also reproduced in our work, but we believe that these structural rearrangements are not sufficient for the

major energetic requirement found experimentally. Our results, in accordance with those of Stackhouse et al.,[11] reveal that the progress of the dehydroxylation reaction does not require a higher activation energy (58−59 kcal/mol for the first step and 60.3 kcal/mol for the second dehydroxylation step). The formation of all of these structures indicates that the dehydroxylation process is much more complex than a first-order reaction and can explain the wide range of temperatures necessary to complete the release of water in this process. These conclusions are thought to be valid for other aluminum-containing dioctahedral 2:1 phyllosilicates.

Acknowledgment. The authors are thankful to D. Martín-Ramos and A. Martín-Islán for the use of XPowder software and to Centro Técnico de Informática of CSIC, centro de Cálculo del CIEMAT, Centro de Cálculo de Galicia (CESGA), and Centro de Supercomputación de la Universidad de Granada for allowing the use of its computational facilities. E.M.-M. is thankful to MEC (FPU Programme) and CSIC (I3P Programme) for financial support. This work was supported by Spanish MCYT and European FEDER Grants CGL2005-02681, BTE2002-03838, and CTQ2004-04648.

References and Notes

(1) Molina-Montes E.; Donadio, D.; Hernández-Laguna, A.; Sainz-Díaz, C. I.; Parrinello, M. *J. Phys. Chem. B* **2008**, *112*, 7051–7060.
(2) Wardle, R.; Brindley, G. W. *Am. Mineral.* **1972**, *57*, 732–750.
(3) Fitzgerald, J. J.; Hamza, A. I.; Dec, S. F.; Bronnimann, C. E. *J. Phys. Chem.* **1996**, *88*, 6206–6209.
(4) McKenzie, J. K. D.; Brown, I. W. M.; Meinhold, R. H.; Bowdem, M. E. *J. Am. Mineral. Ceram. Soc.* **1985**, *68*, 266–272.
(5) Mazzucato, E.; Artioli, G.; Gualtieri, A. *Phys. Chem. Miner.* **1999**, *26*, 375–385.
(6) Wang, L.; Zhang, M.; Redfern, S. A. T.; Zhang, Z. *Clays Clay Miner.* **2002**, *50*, 272–283.
(7) Drits, V. A.; Besson, G.; Muller, F. *J. Phys. IV* **1996**, *C4*, 91–102.
(8) Kloprogge, J. T.; Kamarneni, S.; Yanagirawa, K.; Fry, R.; Frost, R. L. *J. Colloid Interface Sci.* **1999**, *212*, 562–569.
(9) Heller, L.; Farmer, V. C.; Mackenzie, R. C.; Mitchell, B. D.; Taylor, H. F. W. *Clay Miner. Bull.* **1962**, *5*, 56–72.
(10) Guggenheim, S.; Chang, Y.-H.; Koster van Gross, A. F. *Am. Mineral.* **1987**, *72*, 537–550.
(11) Stackhouse, S.; Coveney, P. V.; Benoit, D. M. *J. Phys. Chem. B* **2004**, *108*, 9685–9694.
(12) Ogloza, A. A.; Malhotra, V. M. *Phys. Chem. Miner.* **1989**, *16*, 378–385.
(13) Malhotra, V. M.; Ogloza, A. A. *Phys. Chem. Miner.* **1989**, *16*, 386–393.
(14) Sainz-Díaz, C. I.; Timón, V.; Botella, V.; Hernández-Laguna, A. *Am. Mineral.* **2000**, *85*, 1038–1045.
(15) Sainz-Díaz, C. I.; Timón, V.; Botella, V.; Artacho, E.; Hernández-Laguna, A. *Am. Mineral.* **2002**, *87*, 958–965.
(16) Sainz-Díaz, C. I.; Escamilla-Roa, E.; Hernández-Laguna, A. *Am. Mineral.* **2004**, *89*, 1092–1100.
(17) Bray, H. J.; Redfern, S. A. T. *Mineral. Mag.* **2000**, *64*, 337–346.
(18) *CPMD*, version 3.9.2; IBM Corp. and MPI fuer Festkoerperforschung: Stuttgart, Germany, 2004.
(19) Becke, A. D. *Phys. Rev. A* **1988**, *38*, 3098–3100.
(20) Lee, C.; Yang, W.; Parr, G. M. *Phys. Rev. B* **1988**, *37*, 785–789.
(21) Troullier, N.; Martins, J. L. *Phys. Rev. B* **1991**, *43*, 1993–2006.
(22) Car, R.; Parrinello, M. *Phys. Rev. Lett.* **1985**, *55*, 2471–2474.
(23) Laio, A.; Parrinello, M. *Proc. Natl. Acad. Sci. U.S.A.* **2002**, 12562–12566.
(24) Iannuzzi, M.; Laio, A.; Parrinello, M. *Phys. Rev. Lett.* **2003**, *90*, 238302.
(25) Laio, A.; Rodriguez-Fortea, A.; Gervasio, F.; Ceccarelli, M.; Parrinello, M. *J. Phys. Chem. B* **2005**, *109*, 6676.
(26) Hamilton, T. P.; Pulay, P. *J. Phys. Chem.* **1986**, *84*, 5728–5734.
(27) Billeter, S. R. Curioni A., Andreoni W. *Comput. Mat. Sci.* **2003**, *27*, 437–445.
(28) Banerjee, A.; Adams, N.; Simons, J.; Shepard, R. *J. Phys. Chem.* **1985**, *89*, 52–57.
(29) Udagawa, S.; Urabe, K.; Hasu, H. *Jpn. Assoc. Mineral. Petrol. Econ. Geol.* **1974**, *69*, 381–389.
(30) Frost, R. L.; Barron, P. F. *J. Phys. Chem.* **1984**, *88*, 6206–6209.
(31) Giese, R. F. *Clays Clay Miner.* **1979**, *27*, 213–223.
(32) Leffler, J. E. *Science* **1953**, *117*, 340.
(33) Hammond, G. S. *J. Am. Chem. Soc.* **1955**, *77*, 334.
(34) Bickmore, B. R.; Rosso, K. M.; Nagy, K. L.; Cygan, R.T.; Tadanier, C. J. *Clays Clay Miner.* **2003**, *51*, 359–371.
(35) Martín-Ramos, J. D. *Using XPowder: A Software Package for Powder X-Ray Diffraction Analysis*; June, 2004; available at http://www.xpowder.com.

JP8010876